Supplementary material

S1. Pumping effect of moving microsphere

Microspheres are moving through an aqueous solution in the Stokes flow regime. For a moving microsphere the drag force is known as:

$$F_\mathrm{d} = 6 \ \pi \ \eta_\mathrm{w} \ r_\mathrm{d} \ u_\mathrm{m} \tag{S1.1}$$

where η_w is the viscosity of the liquid, r_d the radius of the microsphere and u_m the velocity of the microsphere.
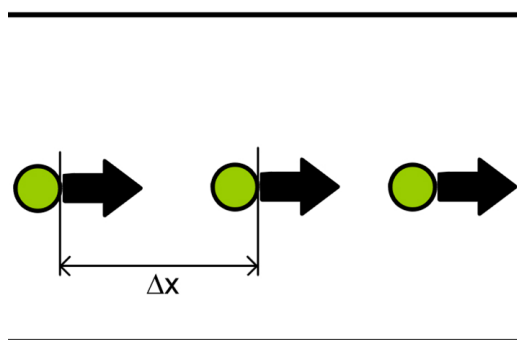

Figure S1.1: a series of microspheres moving with a separation distance Δx

This drag force of a series of moving microspheres is exerted on the fluid as shown in Figure S1.1 and Equation S1.1, generating a pressure difference Δp in the channel:

$$\Delta p = \frac{F_\mathrm{d}}{h \ w} \tag{S1.2}$$

Where h is the height and w the width of the microchannel. This pressure difference is generated in every unit cell having a length of Δx. In flat microchannels the average fluid flow (u_c) can be written as [2]

$$\overline{u_\mathrm{c}} = \frac{h^2}{12 \ \eta_\mathrm{w}} \frac{\Delta p}{\Delta x} \tag{S1.3}$$

with Equations S1.1, S1.2 and S1.3, the ratio between the average channel fluid velocity $\overline{u_c}$ and the microsphere velocity u_m can be calculated

$$\eta_\mathrm{m \to c} = \frac{\overline{u_\mathrm{c}}}{u_\mathrm{m}} = \frac{\pi \ h \ r_\mathrm{d}}{2 \ w \ \Delta x} \tag{S1.4}$$

This approximation gives insight in the magnitude and scaling of the generated pumping motion. The ratio of velocities does not depend on the viscosity. A wider channel will decrease the flow rate, since there is more volume to displace. A higher channel will increase the flow rate (less hydrodynamic resistance), the model, however, is only valid under the flat channel approximation. Larger microspheres will displace more fluid, especially when they are placed

1

close to each other (small Δx). A minimum height and width of the channel is determined by the size of the microspheres.

The geometries in our experiment are: channel height $h = 23~\mu m$, channel width $w = 105~\mu m$, microsphere radius of $r_\mathrm{d} = 17~\mu m$ and a separation distance $\Delta x = 95~\mu m$. This results in a velocity ratio $\eta_\mathrm{m \to c}$ of 6%.

S2.   Simulation results of flow rate

Using COMSOL Multiphysics 4.2a the flow was simulated using a 2D model. The Fluid-Structure Interaction physics module and incompressible flow neglecting the inertial terms were used.
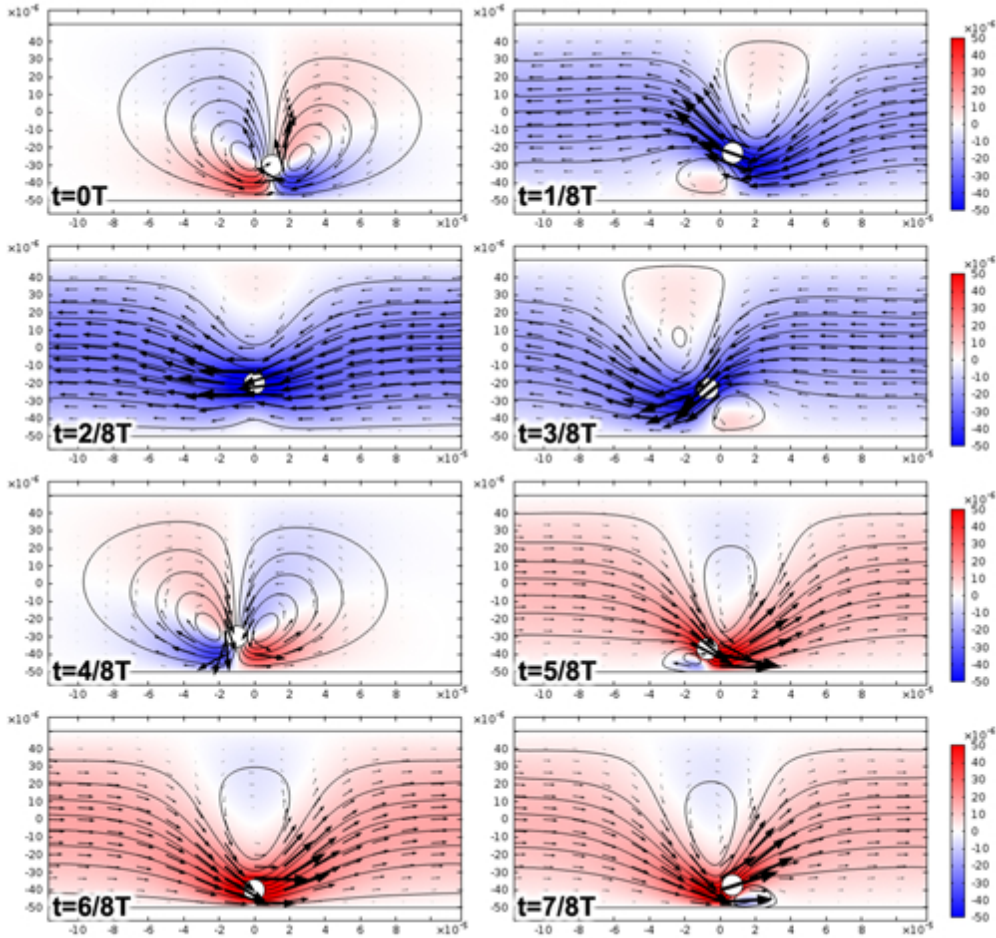

Figure S2.1: 2D simulation of the Stokes flow around a circle making a circular motion in the microchannel. The color indicates the magnitude of the flow in horizontal direction, the arrows indicate the direction of the flow.
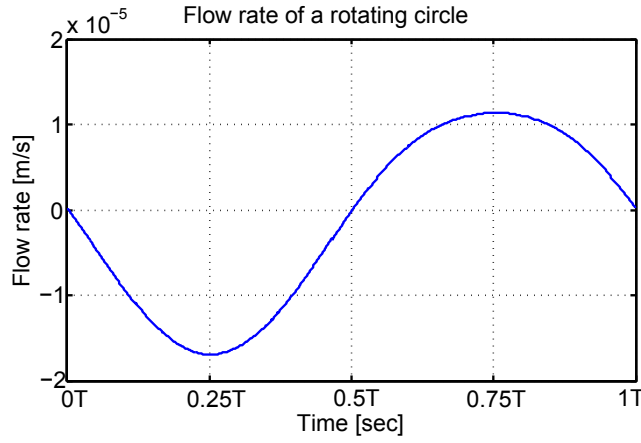
Figure S2.2: The output flow rate at the end of the simulated cell. This flow rate was calculated by integrating the velocity over the right boundary and dividing by the boundary length ($1/w \int_{width} u_x \, dy$). It can be seen that there is a clear asymmetry in the flow rate. This simulation model results in a pumping efficiency $\eta_{\mathrm{m \to c}}$ of 33%.

S3. Magnetic properties of the permalloy

Figure S3.1 shows the magnetic hysteresis loop of the 480 nm continuous permalloy ($\mathrm{Ni_{80}Fe_{20}}$ film), similar to the one used to fabricate the disks. The peculiar shape of the loop is due to stripe domains, which is typical for permalloy film of this thickness. These stripe domains are caused by an out-of-plane component in the anisotropy [1], most likely caused by crystalline growth with a preferred orientation. Even though the susceptibility is far from optimal, these films reach a magnetisation of about 75% of their saturation value of 790(50) kA/m at the field of 24 mT applied in the experiments.
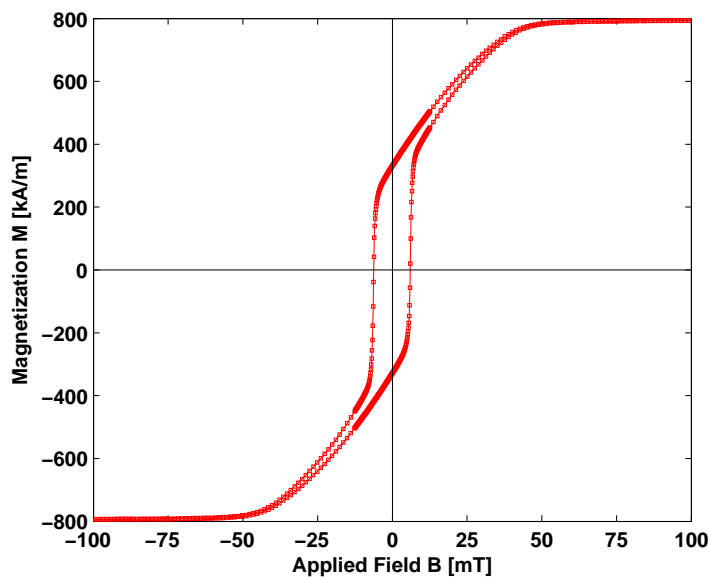

Figure S3.1: The magnetization curve of the permalloy disks, showing saturation at about 800 kA/m for fields above 50 mT.

S4. Dipole field approximation

The stray field of magnetic disc of radius r_d and thickness t_d, saturated to its saturation magnetisation M_s, can be approximated by a magnetic line charge with charge density

$$\lambda = M_s t \cos\theta \quad [\text{A}], \tag{S4.5}$$

where θ is as defined in figure S4.1. This approximation is correct for points that lie much further from the edge of the disc than its thickness ($r - r_d \gg t_d$). Integration over infinitesimal charge packages $\lambda r_d d\theta$ yields for the magnitude of the magnetic field $\boldsymbol{B}$ at location $\boldsymbol{r}$ in figure S4.1

$$B = \frac{\mu_0 M_s t}{2\pi r_d} \int_0^\pi \frac{(x - \cos\theta)\cos\theta}{(x^2 - 2x\cos\theta + 1)^{(3/2)}} d\theta \quad [\text{T}] \tag{S4.6}$$

with $x = r/r_d$. The integral was solved numerically, and compared to the field of a point dipole with a moment equal to the volume of the disk times the saturation magnetisation

$$B_{\text{dip}} = \frac{\mu_0 M_s t}{2 r_d} \frac{1}{x^3}. \tag{S4.7}$$

The ratio between the line charge approximation and the dipole field is shown in figure S4.1. For $r > 3r_d$ the error made by using a dipole approximation is less than 10%.
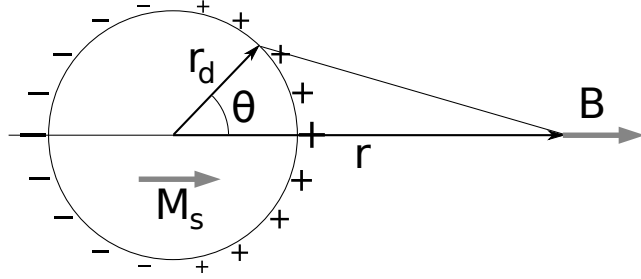

Figure S4.1: The magnetic field of a saturated disc can be approximated by a line charge, with a charge density proportional to $\cos\theta$.
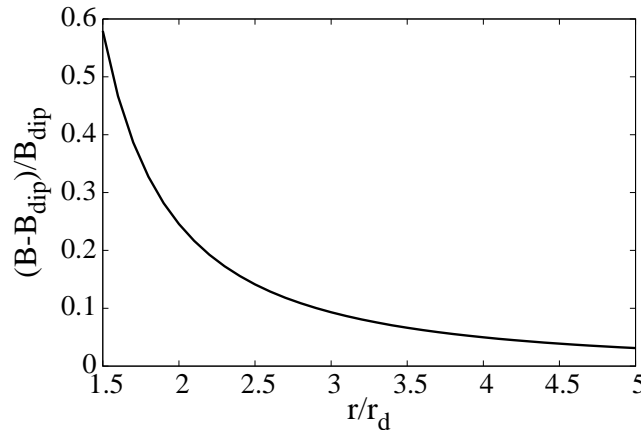

Figure S4.2: The error made by assuming the disc to be a dipole as a function of the distance from the center of the disc.

Bibliography

[1] J. McCord, B. Erkartal, T. Von Hofe, L. Kienle, E. Quandt, O. Roshchupkina, and J. Grenzer. Revisiting magnetic stripe domains - anisotropy gradient and stripe asymmetry. *Journal of Applied Physics*, 113(7), 2013. cited By 1.

[2] R. E. Oosterbroek. *Modeling, design and realization of microfluidic components.* Universiteit Twente, 1999.